Available online at www.sciencedirect.com

ScienceDirect

Procedia Engineering 147 (2016) 56 – 61

Procedia Engineering

www.elsevier.com/locate/procedia

11th conference of the International Sports Engineering Association, ISEA 2016

Experiment of aerodynamic force on a rotating soccer ball

Sungchan HONG, Ryosuke NOBORI*, Keiko SAKAMOTO

Masaaki KOIDO, Masao NAKAYAMA,Takeshi ASAI

University of Tsukuba, Tsukuba-city, Ibaraki, 305-8574, Japan.

Abstract

The purpose of this study was to measure the aerodynamic force acting upon a soccer ball spun in a wind-tunnel test. In particular, we prepared two types of spinning soccer balls (air and motor types), measured the aerodynamic force on each, and examined the validity of the measurement method. In the case of the air-type spinning ball, the ball was made to spin by applying compressed air from an air compressor via an air duster. In the case of the motor-type spinning ball, a motor was placed at the middle inside the ball, and the ball was then automatically spun. First, both the air- and motor-type spinning balls demonstrated very strong spin-parameter (*Sp*) dependence with respect to drag during spinning. In addition, the side-force coefficient showed signs of linear increase as *Sp* increased in the motor-type spinning ball, whereas it increased along a slight curve in the air-type spinning ball. In particular, a negative Magnus effect was observed in the motor-type spinning ball when the Reynolds number was approximately 2.0×10^5 and *Sp* was approximately 0.14 (-0.007) and when the Reynolds number was approximately 2.2×10^5 and *Sp* was approximately 0.13 (-0.005).

Peer-review under responsibility of the organizing committee of ISEA 2016

Keywords: Aerodynamics; Ball; Soccer; Trajectory

1. Introduction

A number of studies have been conducted in recent years on the aerodynamic and flight characteristics of soccer balls due to changes in the form of the ball panels [1-7]. However, these studies were mainly concerned on the aerodynamic characteristics of fixed non-spinning soccer balls and did not elucidate the aerodynamic characteristics of curving or otherwise spinning soccer balls most often used in soccer matches. The major reasons for this deficiency are the extreme difficulty in spinning balls and the fact that obtaining precise data from the influence of auxiliary tools (wires and frames) needed to provide spin is believed to be difficult. However, kicking a non-spinning ball during a soccer match [8,9], including balls demonstrating a knuckling effect [10-12], is actually an extremely difficult technique and very infrequently occurs. In other words, most soccer balls in flight spin in various directions, and we believe that the fundamental state of a ball flying during an actual match is spinning. Therefore, in this study, we prepared two types of spinning soccer balls (air and motor types) to measure the aerodynamic forces on a soccer ball in the wind tunnel and examined the aerodynamic characteristics of the spinning soccer balls from the obtained aerodynamic force data. In addition, by comparing the aerodynamic force on the two types of spinning soccer balls used in the tests, we examined the validity of each measurement model.

* Ryosuke Nobori. Tel.: +81-29-853-6318.
E-mail address: nobohoudaicare@yahoo.co.jp

Peer-review under responsibility of the organizing committee of ISEA 2016
doi:10.1016/j.proeng.2016.06.189

2. Methods

2.1. Wind-tunnel test

In this test, we used a closed-circuit, low-speed, and low-turbulence wind tunnel in the University of Tsukuba, Japan (Fig. 1). The maximum wind speed was 55 m/s, the blow-off size was 1.5 m × 1.5 m, the wind-speed distribution was within ±0.5%, and the turbulence was 0.1% or less. The test was performed by mounting four types of soccer balls in this wind tunnel as test subjects. In addition, the force acting on the soccer balls was measured by a sting-type six-component force detector (LMC-61256, Nissho Electric Works). The data obtained from the test were recorded by a computer via an A/D conversion board.

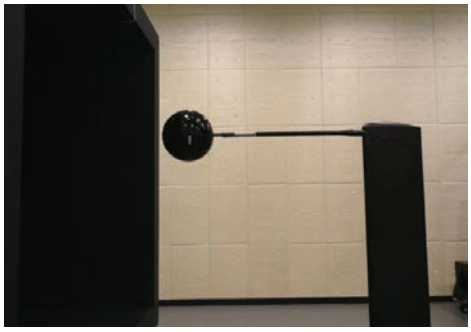

Fig. 1. Wind-tunnel test setup.

In this test, the drag coefficient (C_D) and side-force coefficient (C_S) were obtained from the measured aerodynamic force [Equations (1) and (2)]. In addition, the spin parameter (Sp) was used for the dimensionless relationship between the spin and speed.

$$Cd = \frac{2D}{\rho U^2 A} \quad (1)$$

$$Cs = \frac{2S}{\rho U^2 A} \quad (2)$$

Here, ρ is the air density (ρ = 1.2 kg/m^3). U is the flow rate (in meters per second). A is the projected area (in square meters) of the soccer ball.

$$Sp = \omega R / U \quad (3)$$

Sp indicates the ratio of the flow rate to the spin speed, ω indicates the angular speed, R indicates the ball radius, and U indicates the flow rate.

In this study, two types of balls were used in the test: air- and motor-type balls (Fig. 2).

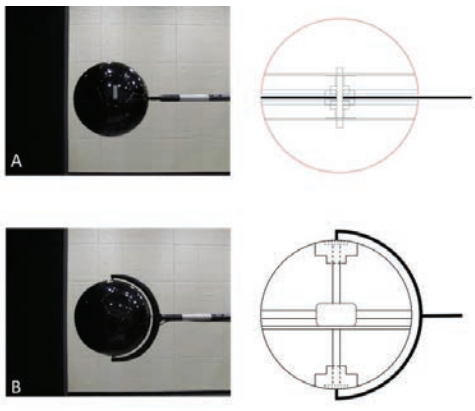

Fig. 2. Setup of the spinning soccer ball used in this test. (a) Air-model design drawing. (b) Motor-model design drawing.

In this study, we used the typical 32-panel soccer balls (with 12 pentagonal and 20 hexagonal panels) for the spinning and non-spinning tests. In addition, the air-type ball was a fibre-reinforced plastic ball, which is broadly divided into three constituent parts: the top hemisphere, the middle, and the bottom hemisphere. The middle part was connected to the sting of the wind tunnel and, thus, did not spin. In addition, the air-type ball was spun by providing compressed air from an air compressor via an air duster. The spin rate was assumed to be within the range of from 2 to 8 rps in which the spinning was relatively stable. The spin rate was obtained by detecting the spinning of a marker attached to part of the spinning ball using a tachometer.

On the other hand, the motor-type soccer ball involved the installation of a motor within the ball to provide motive power for spinning and then spins the ball through a power transmission disk. The motor within the ball was connected to a control panel outside the ball via an electronic cable, and this panel was used to maintain a constant spin rate. The spin rate was set to be from 3 to 8 rps in which the spinning was relatively stable. At 2 rps, the spinning was not stable and was thus considered to be outside the scope of measurements of the motor-type ball. The sampling frequency for each measurement data was 1 kHz. The measurements were made every 10-s period, and the mean value was considered as the steady-state measurement value.

3. Results

In this study, we measured the drag and side force under spinning and non-spinning conditions in the wind tunnel and used the obtained data to calculate the drag and side coefficients.

3.1. Drag coefficient of the balls under non-spinning condition

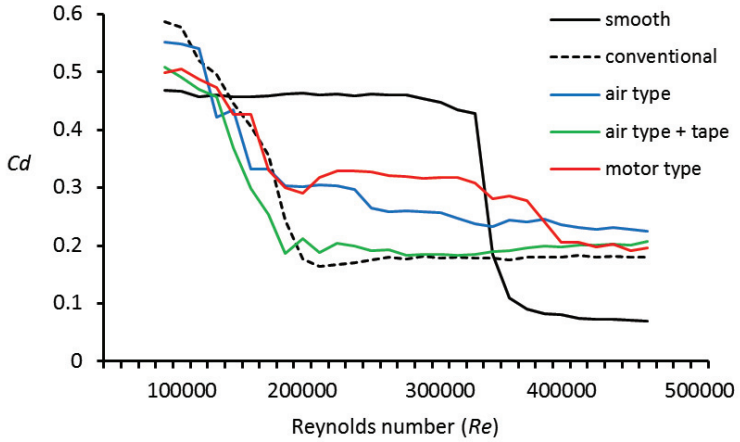

Fig. 3. Drag coefficient variation by model types under non-spinning condition.

We calculated the drag coefficient of various balls under non-spinning condition using the wind-tunnel test (Fig. 3). We observed that the drag significantly varied with the ball type. The critical Reynolds numbers for a conventional ball (Molten, 32-panel) were determined to be 2.2×10^5 (0.16), which are similar to previous tests [1-3]. When we observed *Cd* of the air-type ball, *Cd* showed signs of decreasing from a maximum value of approximately 0.47 to a minimum value of approximately 0.23 as the Reynolds number increased. In addition, when tape correction (for the tests in which the gap present in the middle of the ball is covered with tape) was performed, the drag coefficient changed within the range of approximately from 0.5 to 0.2, and the critical Reynolds number was approximately 2.1×10^5 (0.18). We assume that this result can be attributed to some types of effect from the gap existing in the middle of the air-type ball.

In addition, *Cd* of the motor-type ball decreased from the start of measurement, reached approximately 0.29 with a Reynolds number of approximately 2.0×10^5, and thereafter showed a slight increase but then appeared to again decrease with a Reynolds number of approximately 3.4×10^5. Thus, the critical Reynolds number was approximately 2.0×10^5 (0.2). We assume that this occurrence was due to the effect on the ball slipstream at the top-to-bottom axle installed to support the motor-type ball. Thus, a further step in the future to examine the effect of the axle that supports the ball is needed via visualization test using particle image velocimetry.

3.2. Drag coefficient of the air-type ball under spinning condition

When we observed the relationship between the drag coefficient and *Sp* of the air-type spinning soccer ball, *Cd* appeared to increase as *Sp* increased (Fig. 4). However, it was observed to momentarily decrease at low speeds (10 m/s or less). In the latest studies of spinning soccer balls, *Cd* of a spinning ball reportedly decreased between *Sp* of approximately from 0.26 to 0.51 and a Reynolds number of approximately 0.96×10^5 [13]. These results matched the region in which *Cd* was observed to decrease in

our tests. In addition, Asai et al. [14] reported that *Cd* linearly increased as *Sp* increased within an *Sp* range of approximately from 0.05 to 0.3 and a Reynolds number of approximately from 3.1×10^5 to 4.6×10^5, indicating a similar increase to our tests.

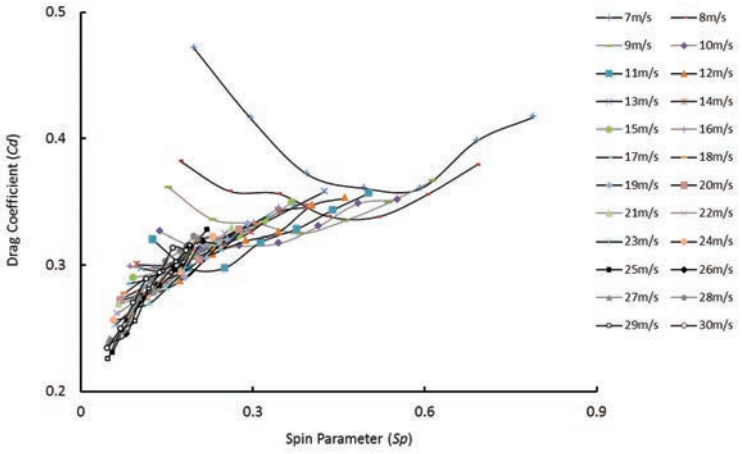

Fig. 4. Relationship of the drag coefficient and *Sp* on the air-type spinning soccer ball.

3.3. Drag coefficient of the motor-type ball under spinning condition

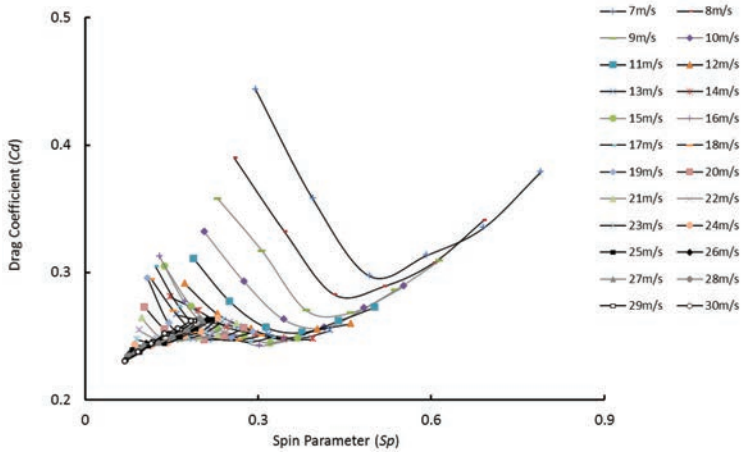

Fig. 5. Relationship of the drag coefficient and *Sp* on the motor-type spinning soccer ball.

With regards to the relationship between *Cd* and *Sp* of the motor-type spinning ball (Fig. 5), we confirmed that the drag coefficient decreased in the low-speed regions, which was similar to that of the air-type spinning ball. However, the decrease in *Cd* of the motor-type spinning ball not only occurred in the low-speed region but also extended to the medium-speed regions. In addition, Kim et al. [15] reported that, similar to our tests, *Cd* decreased in the spinning tests involving a smooth ball. However, because we do not know whether this result is due to the axle behind the motor-type spinning ball, a pending issue would be the visualization of the air flow on the ball surface.

3.4. Side-force coefficient of the air-type ball under spinning condition

With regards to the relationship between the side-force coefficient and *Sp* of the air-type spinning soccer ball (Fig. 6), *Cs* increased as *Sp* increased at all wind speeds due to the Magnus effect. The same tendency was observed in previous studies

[13,14]. However, Asai et al. [14] reported that *Cs* was approximately 0.29 when the Reynolds number was approximately 3.3 × 10^5 and *Sp* was approximately 0.2 in a study of a Teamgeist ball. This result was approximately 0.05 lower than the *Cs* in the same region in our tests (approximately 0.24). Furthermore, lower values were observed in all other regions. This difference in the results is believed to be due to the effect of the gap present in the air-type spinning ball and the differences in the shape of the soccer balls used in the test.

In addition, Kray et al. [13] reported that a negative Magnus effect occurred in which minimum *Cs* was approximately -0.09 when the Reynolds number was approximately 2.06 × 10^5 and *Sp* was approximately 0.06. In addition, A negative Magnus effect (-0.3) was reported when the Reynolds number was approximately 0.9 × 10^5 and *Sp* was approximately from 0.1 to 0.2 [15]. However, in our tests, *Cs* was not observed to decrease as *Sp* increased.

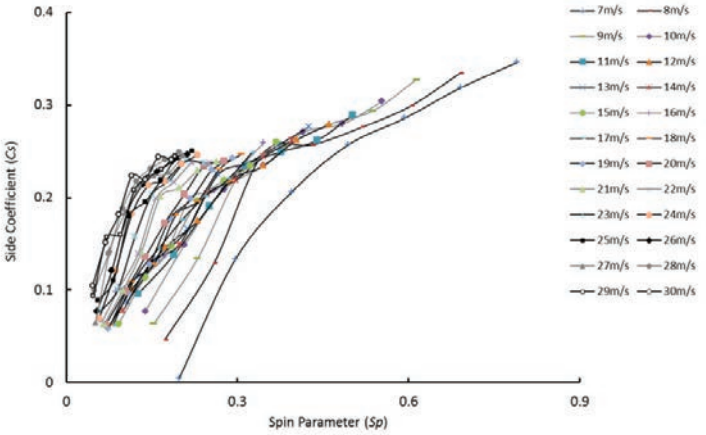

Fig. 6. Relationship of the side-force coefficient and *Sp* on the air-type spinning soccer ball.

3.5. Side-force coefficient of the motor-type ball under the spinning condition

With regards to the relationship between *Cs* and *Sp* of the motor-type spinning ball (Fig. 7), an increase in *Cs* appeared to occur in most regions as *Sp* increased, similar to that of the air-type spinning ball, due to the Magnus effect. However, *Cs* was observed to decrease for wind speeds of 7 m/s (approximately from 0.30 to 0.39) and 8 m/s (approximately 0.26 to 0.35). In addition, *Cs* showed negative values (on the order of -0.007 and -0.005) when the motor-type spinning ball Reynolds number was approximately 2.0 × 10^5 and *Sp* was approximately 0.14 and when the Reynolds number was approximately 2.2 × 10^5 and *Sp* was approximately 0.13. These results were the same as those in the negative Magnus-effect region [14,16].

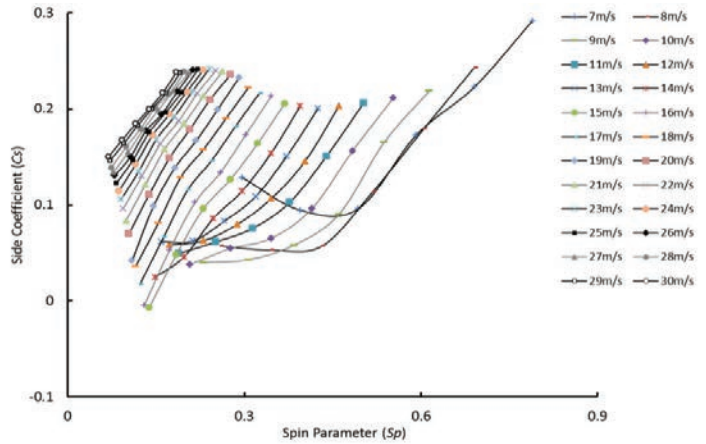

Fig. 7. Relationship of the side-force coefficient and *Sp* on the motor-type spinning soccer ball.

4. Conclusion

In this study, we used air- and motor-type spinning balls to examine the drag and side force during spinning of a soccer ball. First, although the drag values of the air- and motor-type spinning balls differed, both linearly increased as *Sp* increased.

However, the side force was observed to decrease in the low-speed regions. Furthermore, in the case of the motor-type spinning ball, the side force in the medium-speed regions displayed negative values.

In addition, in the method used in this study, the results were greatly affected by the gap in the air-type spinning ball and the axle behind the motor-type spinning ball. Hence, although we failed to determine which method was better, we were able to confirm their individual characteristics. Our future work will be to examine the air flow of the ball slipstream using visualization tests to address the limitations of the present study.

References

[1] Alam, F. et al., A comparative study of football aerodynamics, Procedia Eng, 34: 146–151. 2012.
[2] Goff, J.E., Asai, T., and Hong, S., A comparison of Jabulani and Brazuca non-spin aerodynamics, Proceedings of the Institution of Mechanical Engineers, Part P: J. Sports Eng. Technol, 228: 188–194. 2014.
[3] Hong. S. and Asai. T., Effect of panel shape of soccer ball on its flight characteristics. Sci. Rep, 4: 5068. 2014.
[4] Hong, S., Asai, T., and Seo, K., Visualization of air flow around soccer ball using a particle image velocimetry. Sci. Rep, 5: 15108. 2015.
[5] Oggiano, L. and Sætran, L., Aerodynamics of modern soccer balls, Procedia Eng, 2: 2473–2479. 2010.
[6] Passmore, M. et al., The aerodynamic performance of a range of FIFA-approved footballs, Proceedings of the Institution of Mechanical Engineers, Part P: J. Sports Eng. Technol, 226: 61–70. 2012.
[7] Rogers, D. et al., An experimental validation method of wind tunnel measurements on FIFA approved footballs using kicking tests in wind-free conditions, Procedia Eng, 2: 2481–2486. 2010.
[8] Hong, S., Chung, C., Sakamoto, K. and Asai, T., Analysis of the swing motion on knuckling shot in soccer, Procedia Eng, 13, 176–181. 2011.
[9] Hong, S., Kazama, H., Nakayama, M., and Asai, T., Ball impact dynamics of knuckling shot in football, Procedia Eng, 34, 200–205. 2012.
[10] Asai, T. and Kamemoto, K., Flow structure of knuckling effect in footballs. J. Fluids Struct. 27, 727–733. 2011.
[11] Hong. S., Chung. C., Nakayama. M., and Asai. T., Unsteady aerodynamics force on a knuckleball in soccer. Procedia Eng, 2: 2455–2460. 2012.
[12] Mizota, T. et al., The strange flight behaviour of slowly spinning soccer balls. Sci. Rep, 3, 1871. 2013.
[13] Kray. T., Franke. J., and Frank. W., Magnus effect on a rotating soccer ball at high Reynolds numbers. Journal of Wind Engineering and Industrial Aerodynamics. 124: 46–53. 2014.
[14] Asai. T., Seo. K., Kobayashi. T., and Sakashita. R., Fundamental aerodynamics of the soccer ball. Sports Eng. 10(2): 101–109. 2007.
[15] Kim. J., Choi. H., Park. H., and Yoo. J. Y., Inverse Magnus effect on a rotating sphere: When and why. Journal of Fluid Mechanics. 754: R2 (11 pages). 2014.
[16] Carré. M.J., Goodwill. S.R., Hakke. S.J., Hanna. R.K., and Wilms. J., Understanding the aerodynamics of a spinning soccer ball. Engineering of Sports, 5: 70–76. 2004.